Volume 10, Number 6 (December 2017) p. 1366 – 1395 • ISSN 1983-4195
http://dx.doi.org/10.1590/S1983-41952017000600011

REVISTA IBRACON DE ESTRUTURAS E MATERIAIS
IBRACON STRUCTURES AND MATERIALS JOURNAL

Self-supporting tests in lattice joists subject to negative bending

Ensaios de autoportância em vigotas treliçadas sujeitas a flexão negativa




I. S. STORCH [a]
storch.engcivil@gmail.com

J. G. S. DOBELIN [a]
joslaine.dobelin@ucb.org.br

L. C. BATALHA [a]
leticia.cbatalha@hotmail.com

A. L. SARTORTI [a]
artur.sartorti@ucb.org.br

Abstract

During the construction of bridges, cantilever roofs and eaves, assembling formworks and scaffold that will support the slabs is a point of difficulty in the construction phase. Therefore, it is relevant the study of the lattice joists which serve as self-supporting formwork, supporting its weight, the weight of the fresh concrete, the weight of workers and the weight of concreting equipment. The analysis of the bearing capacity of lattice joists subject to negative bending with base concrete opening enables checking the maximum span that each lattice truss model bears, either cantilevered or between continuous spans with reduced or no scaffold. The concrete opening enables the monolithism between the slab and its support. This paper presents the results of tests on lattice joist with concrete opening. By the results analysis, formulations for designing the spacing between prop lines were found. The results are promising and indicate great possibilities of using lattice joists with concrete opening over the supports (beams), in order to optimize the slab shuttering.

Keywords: self-supporting, shuttering, negative bending, lattice joist, mini lattice panel, buckling.

Resumo

Em construção de pontes, marquises e beirais, uma das dificuldades encontradas é a montagem de formas e escoramento que darão apoio à laje na fase construtiva. Portanto, apresentam-se relevantes os estudos de vigotas treliçadas que servem como formas autoportantes, suportando, além de seu peso, o peso do concreto fresco, de operários e equipamentos de concretagem. A análise da capacidade portante das vigotas treliçadas sujeitas à flexão negativa com abertura no concreto da base, possibilita a verificação do vão máximo que cada modelo de armadura treliçada suporta em balanço ou entre vãos contínuos com reduzido ou nenhum escoramento. A abertura de concretagem possibilita o monolitismo entre a laje e o seu apoio. Neste artigo são apresentados os resultados de ensaios em vigotas treliçadas com abertura de concretagem na base. Com a análise dos resultados realizada foram encontradas as formulações que permitem o dimensionamento do espaçamento entre linhas de escora. Adianta-se que os resultados encontrados são promissores e indicam grandes possibilidades da utilização de vigotas treliçadas com abertura de concretagem sobre os apoios (vigas), com o objetivo de otimizar o cimbramento da laje.

Palavras-chave: autoportância, cimbramento, momento negativo, vigota treliçada, minipainel treliçado, flambagem.

[a] *Centro Universitário Adventista de São Paulo, Engenharia Civil, Engenheiro Coelho, SP, Brasil.*

Received: 31 Mar 2016 • Accepted: 28 Apr 2017 • Available Online: 11 Dec 2017

1. Introduction

The manufacturing of lattice slabs started in Brazil after the implementation of the first electroplating machine, using steels grade 600. According to the Brazilian code ABNT NBR 14862 [1], lattice reinforcement is a precast element with a three-dimensional prismatic mold, made of two steel wires in the bottom and one steel wire in the top which form its lower and upper flanges, respectively. These elements are connected by electrofusion to two steel wires, called sinusoid (diagonal bars), following a regular 20 cm spacing, known as step and worldwide standardized. The lattice girders are identified for a TR code followed by two digits that represent its height in centimeters. The last three digits represent respectively the upper flange, sinusoid and lower flange diameters, in millimeters.

The code ABNT NBR 14859-1 [2] regulates the precast lattice joists fabrication (VT) with a base of concrete. The lattice girder partially embedded in the concrete base provides a light element easy to handle, requiring fewer shuttering components according to its self-supporting capacity (SARTORI [3]). The joists can be reinforced or not, depending on its structural demand. These constructive elements are normalized according to ABNT NBR 14859-1 [2]; ABNT NBR 14859-2 [4]; ABNT NBR 14860-1 [5]; ABNT NBR 14860-2 [6]; ABNT NBR 14862 [1] and ABNT NBR 15696 [7], reporting to ABNT NBR 6118 [8]. Figure 1A illustrates a lattice joist cross section. The combination of two or more lattice girders comprises mini panels (Figure 1B) and lattice girder panels (Figura 1C).

Gaspar [10] concluded that the lattice joist bearing capacity during the construction phase, considering sagging moments, is governed by the upper flange buckling. The upper flange is characterized by its diameter and diagonal stiffness. As the vertical forces increase, the upper flange is progressively compressed in bending (sagging moment) possibly causing instability or buckling. It is also argued that the shuttering assembly is necessary so that the structure doesn't achieve its ultimate capacity, minimizing the elements stresses. Terni *et al* [11] developed researches using computer programs in order to analyze this behavior in the upper flanges. Sartorti *et al* [3] developed experimental studies with positive bending and shear in lattice joists subject to sagging moments, aiming to provide data about the calculation of spacing between prop lines. It also aimed to obtain a more economic construction process, eliminating issues during the construction phase and ensuring security. The later authors concluded that the element ruin can also be characterized by its diagonal bars buckling – for joists with a height of 25 cm or more – besides the upper flange buckling, which is more frequent in joists with 20 cm height or less.

In another occasion, Sartorti *et al* [9] affirmed that the following situations shall be considered for a self-supporting structure calculation in the ultimate limit state: the upper flange buckling due to sagging moments, the lower flange buckling due to hogging moments, the sinusoid shear buckling, failure for excessive plastic deformation of the tension bars and failure of the welded node due to shear. For the serviceability limit states, the calculation of this elements shall consider the analysis of its vertical displacements.

The assemblage of formwork and shuttering elements is a challenge during the construction of bridges and overpasses. Regarding to this issue, the use of lattice elements is an interesting solution whereas its concrete base works as a self-supporting formwork for the slabs. The reinforcement composing the lattice trusses helps bearing the forces acting in the structure in the serviceability state. The use of these latticed elements dispense the need of many transportation

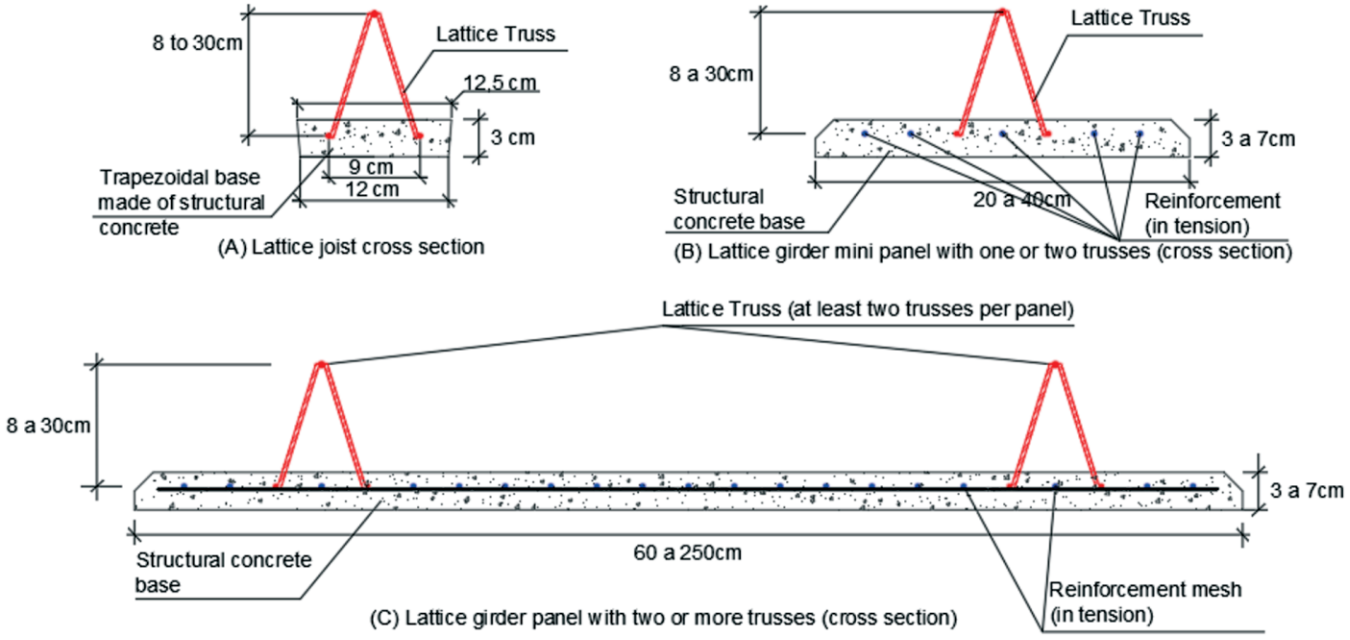

Figure 1
Lattice girder joist and lattice girder panels (cross section scheme)
Source: *Adapted from SARTORTI* et al *[9]*

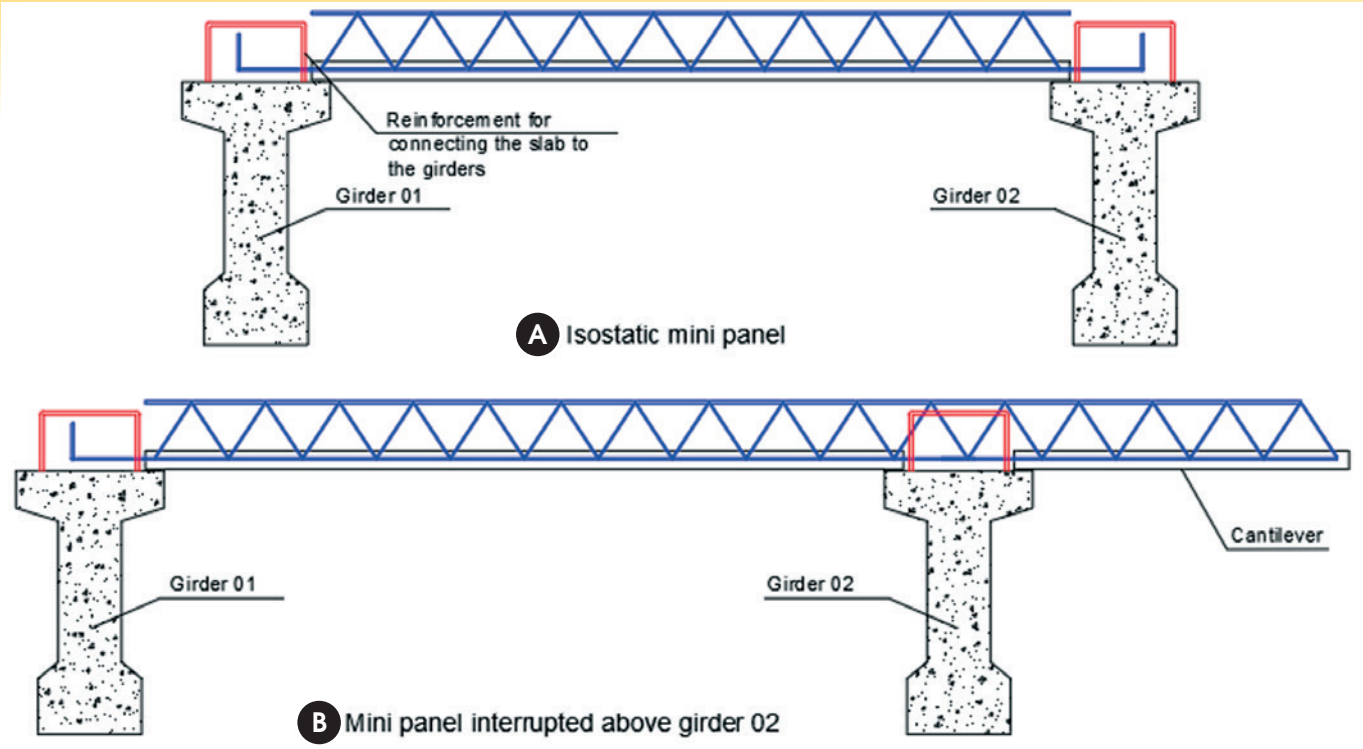

Figure 2
Usual kinds of mini panels used for bridge decks
Source: *SARTORTI* et al *[9]*

equipment, making it easy to handle. This combination of factors results in sustainability and cost saving.

Self-supporting lattice slabs can be used usually in two different manners: simply supported, according to Figure 2A, or with discontinuous concrete joists – particularly the joist located over the supports – making it possible a monolithic joining between the bridge girder and its deck, as shown in Figure 2B.

This research aimed to expand the knowledge concerning self-supporting lattice joists, analyzing its behavior when subject to negative bending and concrete opening (discontinuous concreting) over the supports (Figure 2B). Therefore, the behavior of the steel bars from the lower flange and sinusoids were analyzed, measuring the maximum load bearing capacity of a lattice joist until the serviceability limit state of excessive deformation and the ultimate limit state of instability of any of the latticed components. It was determined the real effective buckling length necessary to the calculation of the maximum span either in cantilever or between supports with no shuttering.

2. Characteristics of the negative bending tests

This item describes the main characteristics of the experimental program.

2.1 Lattice joists

The models of lattice trusses used for the lattice joists are described in Table 1 and its longitudinal and cross section are illustrated in Figures 1A and 3, respectively. For each truss height (6, 8, 10, 12, 16, 20, 25 and 30 cm) there are nine models – three of them with 20 cm concreting interruption, three of them with 30 cm concreting interruption and other three with 40 cm concreting interruption, in a total of 72 lattice joists.

The concrete bases of the joists were cast using the cement type CP V-ARI, with a self-compacting concrete ratio of

Table 1
Lattice reinforcement characteristics

Lattice reinforcement				
Truss code	Height (cm)	Diameter of the bars (mm)		
		Upper	Sinusoid	Lower
TR 06 644	6	6	4.2	4.2
TR 08 644	8	6	4.2	4.2
TR 10 644	10	6	4.2	4.2
TR 12 644	12	6	4.2	4.2
TR 16 745	16	7	4.2	5
TR 20 745	20	7	4.2	5
TR 25 756	25	7	5	6
TR 30 856	30	8	5	6

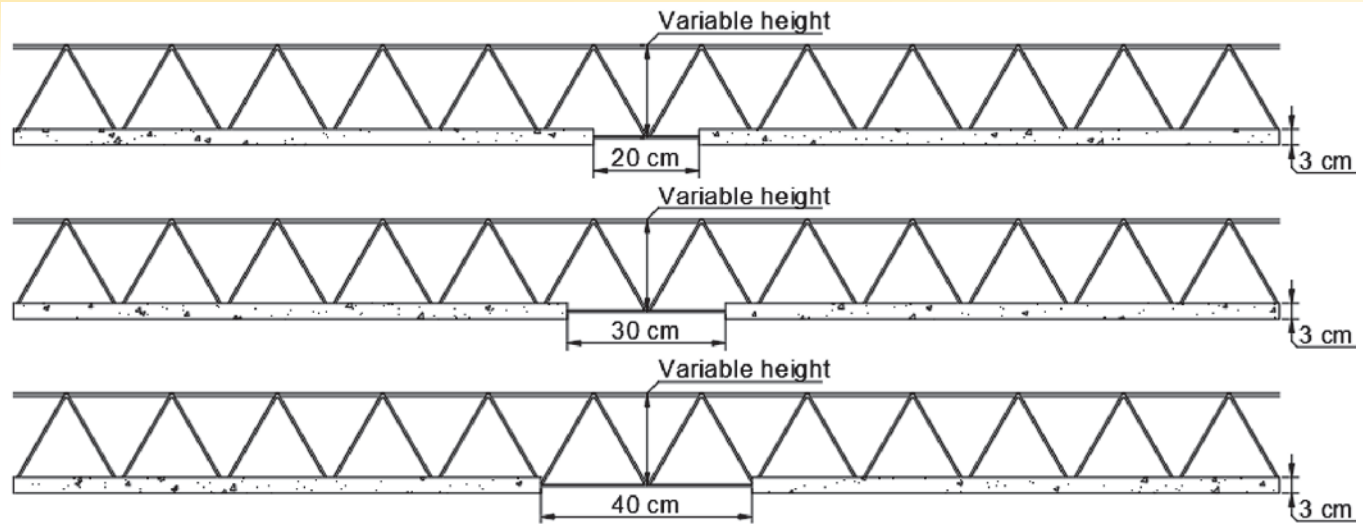

Figure 3
Longitudinal section of the lattice joists models with total length of 240 cm. The concrete opening in the central region in indicated
Source: *Authors*

1:1.526:2.589:0.555:0.375% that are in volume cement: fine sand: stone (type 0): water: superplasticizer, in volume. The base cross section has a width of 12 cm, a height of 3 cm and a length of 240 cm. For the 72 joists, 15 mixtures in a concrete mixer were necessary, regarding to the concrete mixer capacity. Three concrete cylinder tests were conducted for each mix of concrete, expect for the last one, where six concrete cylinders were taken for the determination of the dynamic modulus of elasticity and its characteristic bearing capacity under compression loads.

2.2 Set-up of the bending tests

The bending tests were carried out at a concrete age of 50 days. The following equipment were used: servo-hydraulic universal testing machine (1000 kN capacity); dial indicators with a stroke of 50 mm and a precision of 0.01 mm; magnetic supports for the dial indicators; steel beam used as struts and wood elements used for loading.
The joists were positioned with its upper flange downwards and put above wooden supports which served as pinned supports located

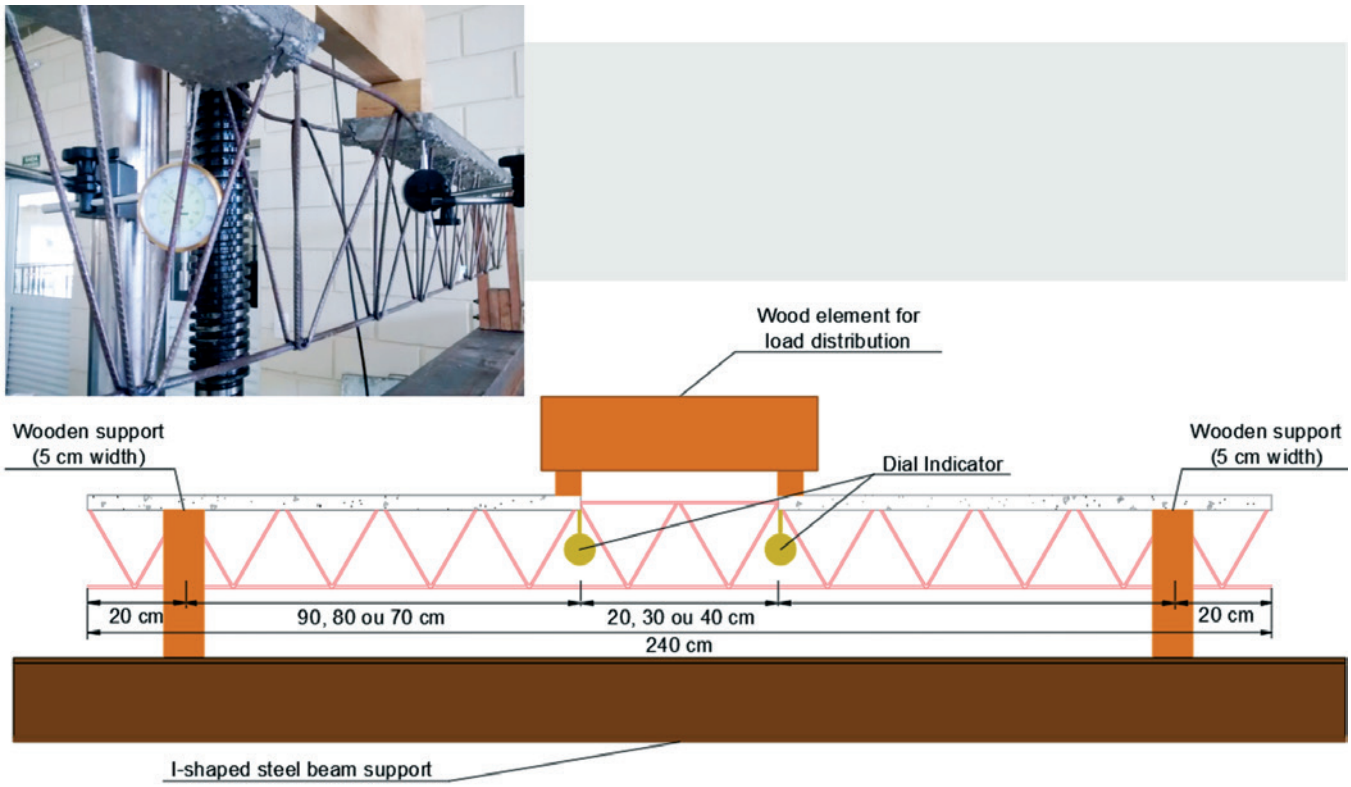

Figure 4
Test set-up: positioning of joists, devices for bending test and dial indicators

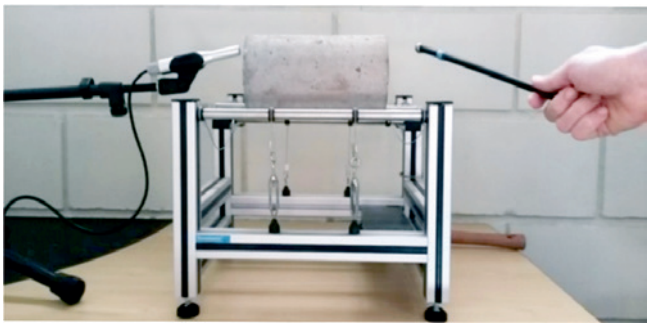

Figure 5
Sonelastic® test set-up: specimen positioning

at 20 cm from the edges of the joist. These wood elements were supported over an I-shaped steel beam. For the distribution of the applied load in two points, two wood pieces were positioned in the edges right before the space where there was no concrete. Five centimeters is a usual value for the width of the bearings of footing under the lattice joists in real structures, what explains the choice of this value for the wood elements width. Vertical displacements due to the loading were measured by two dial indicators (R1 e R2) in the points of loading. The dial indicators were always positioned in the same region in different sides of the joists, according to Figure 4. Displacements due to the self-weight of the lattice joists were not measured. The test set-up is shown in Figure 4.

3. Tests results

This item presents the results of concrete cylinder tests and negative bending tests.

3.1 Concrete specimens

The concrete cylinders for each concrete mixture were tested by the age of 50 days, measuring its Young's modulus and compressive strength. The Young's modulus was measured by an acoustic emission non-destructive test. The cylinder is exposed to an impulse which measures the dynamic modulus of elasticity. The Sonelastic® equipment was used for this purpose. Its functioning is quite simple and the tests can be repeated many times as they are not destructive.

For better understanding this equipment functioning, the following steps can be idealized:

a) The weight and geometry of the specimens are measured and registered in the Sonelastic® computer program;
b) The specimen is positioned under the wires in the nodal points of flexional resonance – 0.224L from the edge of the specimen, where L is its length;
c) Using a pre-determined mass impactor, the specimen suffers an impact providing a sound;
d) The impact sound is recorded by an acoustic conventional receptor (microphone). Two natural frequencies (flexional and longitudinal) of the specimen are contained in the sound waves;
e) The computer program performs a Fast Fourier Transform (FFT) in order to identify the natural frequencies of the specimen;
f) Equations from ASTM E1876-1 [12] are used for calculating the modulus of elasticity having the values of the natural frequencies. Emphasis is given for the fact that the modulus of elasticity is a unique property of the material. The difference between flexional and longitudinal frequencies exists only because of the way they are obtained. Figure 5 illustrates the set-up of the described test.

For more information about Sonelastic® it is recommended reading Sartorti [13].

The values obtained by this method are 20% to 40% higher than the ones obtained with static tests, according to Mehta and Monteiro [14]. A great advantage observed from the dynamic tests is the small variability of results, in sharp contrast with the static tests. Figure 6 shows the results of dynamic elasticity modulus for each concrete mixture.

The axial compression test results are presented in Figure 7. Each specimen has a strength value f_{ci}. The mean value for all the specimens is f_{cm}. Fusco [15] indicates an expression for calculating the characteristic strength of a tested concrete (Equation 1):

$$f_{ck} = f_{cm} - 1{,}645.s \quad (1)$$

Where f_{ck} is the characteristic compressive concrete cylinder strength (by the age of 28 days), with 5% probability of being

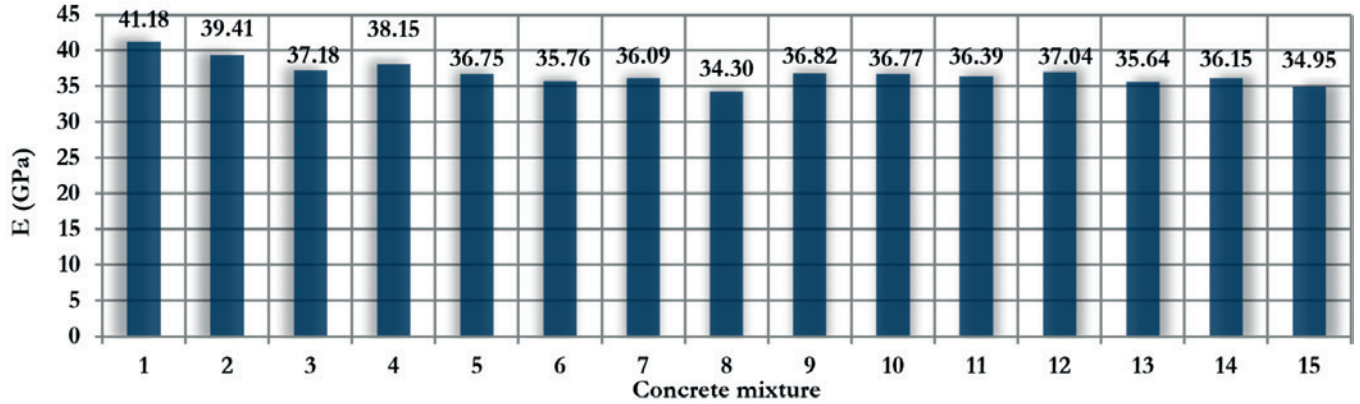

Figure 6
Elasticity modulus test results for each concrete mixture

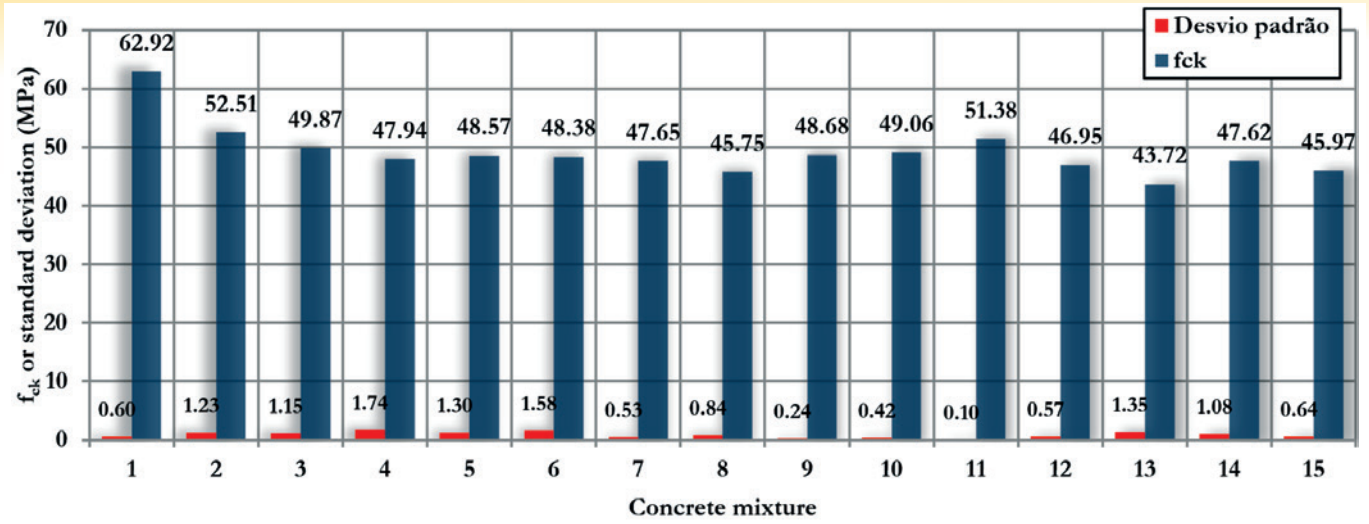

Figure 7
Results of f_{ck} and standard deviation for each concrete mixture

unfavorably exceeded, f_{cm} is the mean concrete compressive strength, s is the standard deviation obtained by $s = f_{cm}.\delta$, and δ is the variance defined by Equation 2, with N = total number of specimens.

$$\delta = \sqrt{\left(\frac{1}{N}\right).\sum_{i=1}^{N}\left[\frac{(f_{ci} - f_{cm})}{f_{cm}}\right]^2} \qquad (2)$$

A variation of f_{ck} results between different concrete mixtures was observed, even when the same ratio was used for the mixes. A small number of cylinder specimens were available for each mixture (equipment limitation), the high room temperature and the low air humidity are some of the reasons attributed by the authors to this variation. Therefore, the different range of time for molding the specimens shall have occasioned the loss of kneading water for the atmosphere, increasing the f_{ck} results variation.

3.2 Negative bending test results

Each of the bending tests resulted in a load *versus* vertical displacement curve, as shown in Figure 8. There were obtained two important parameters: the maximum joist load bearing capacity and the maximum load that corresponds to the maximum displacement.

4. Analysis of results

The analysis of the lattice joists tests aims to define a real effective buckling length for the elements which failure during the test set-up (see Table 2).

After defining the real effective length of joists, mini panels and trussed panels it is possible to use this results in designing situations, in cases when the structural element has a concrete opening and is subject to hogging moments in the opening region. Aiming

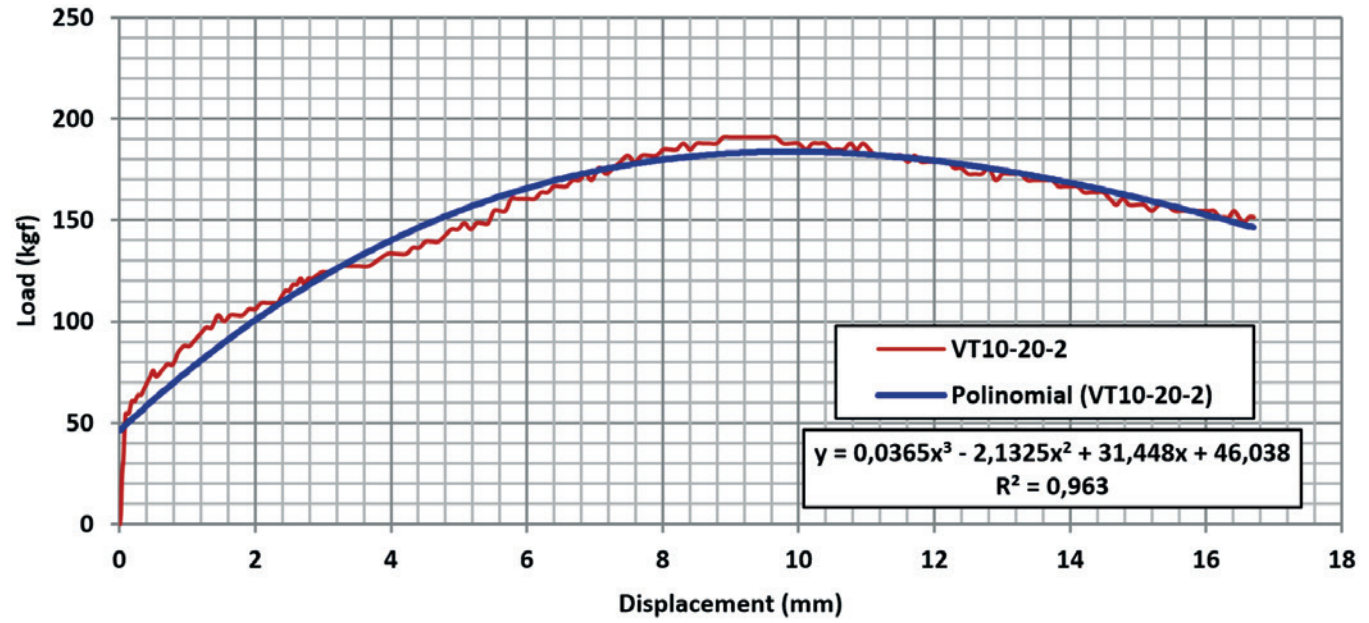

Figure 8
Load *versus* vertical displacement for the VT 20-30-2 joist (lattice joist 10 cm height; concrete opening of 20 cm; second from the three samples tested under the same conditions)

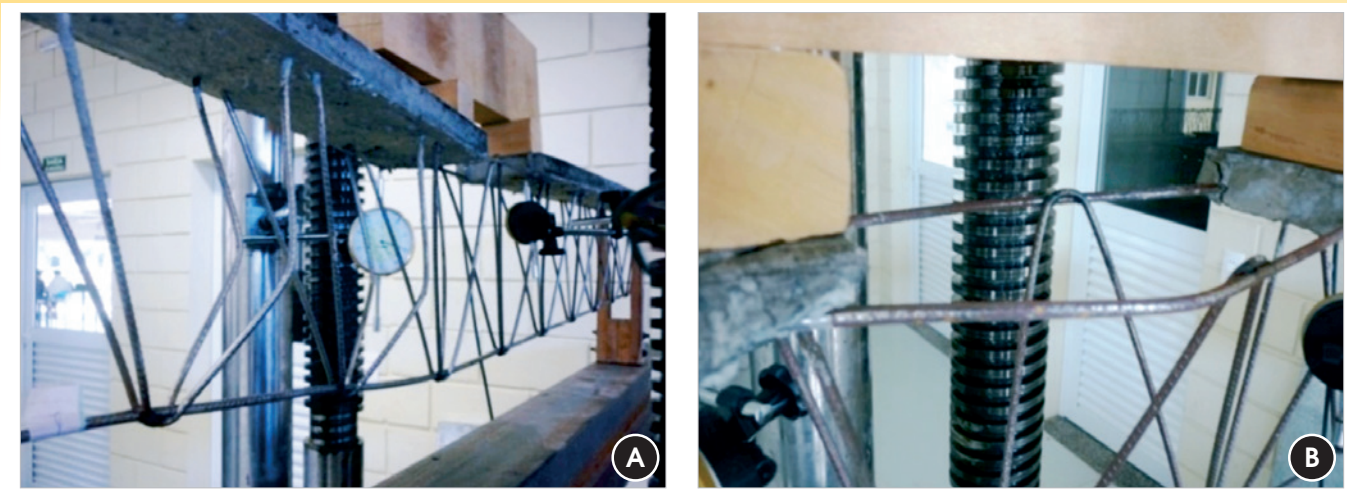

Figure 9
Failure modes: (A) diagonal buckling; (B) lower flange buckling

Table 2
Results for the negative bending tests (Part 1)

Modelo	pp (kN)	PD (kN)	$F_{failure}$ (kN)	F_{limit} (kN)	Failure mode
VT 06 20 1	0.2085	0.036	1.5758	1.0606	Lower flange buckling
VT 06 20 2	0.2085	0.036	1.4242	1.0303	Lower flange buckling
VT 06 20 3	0.2150	0.036	1.4545	1.0303	Lower flange buckling
VT 06 30 1	0.1925	0.036	1.3333	1.0606	Lower flange buckling
VT 06 30 2	0.1935	0.036	1.3030	0.9697	Lower flange buckling
VT 06 30 3	0.1905	0.036	1.2727	0.9697	Lower flange buckling
VT 06 40 1	0.1905	0.036	1.2727	1.0909	Lower flange buckling
VT 06 40 2	0.1785	0.036	1.3636	1.0606	Lower flange buckling
VT 06 40 3	0.1850	0.036	1.0303	0.8485	Lower flange buckling
VT 08 20 1	0.2175	0.036	1.6667	1.4242	Lower flange buckling
VT 08 20 2	0.1990	0.036	1.6970	1.2121	Lower flange buckling
VT 08 20 3	0.2090	0.036	1.9394	1.4545	Lower flange buckling
VT 08 30 1	0.1970	0.036	1.3939	1.1818	Lower flange buckling
VT 08 30 2	0.1940	0.036	1.4242	1.2121	Lower flange buckling
VT 08 30 3	0.1775	0.036	1.3636	1.0909	Lower flange buckling
VT 08 40 1	0.1965	0.036	1.3939	1.2121	Lower flange buckling
VT 08 40 2	0.1815	0.036	1.1818	1.0606	Lower flange buckling
VT 08 40 3	0.1910	0.036	1.3030	1.0606	Lower flange buckling
VT 10 20 1	0.2200	0.036	1.7273	1.3636	Lower flange buckling
VT 10 20 2	0.2175	0.036	1.9091	1.3333	Lower flange buckling
VT 10 20 3	0.2085	0.036	1.6061	1.4545	Lower flange buckling
VT 10 30 1	0.2230	0.036	1.3636	1.2727	Lower flange buckling
VT 10 30 2	Not used due to data error				
VT 10 30 3	0.2055	0.036	1.4242	1.2727	Lower flange buckling
VT 10 40 1	0.1940	0.036	1.2727	1.2121	Lower flange buckling
VT 10 40 2	0.1650	0.036	1.5152	1.4242	Lower flange buckling
VT 10 40 3	0.1955	0.036	1.3030	1.2424	Lower flange buckling
VT 12 20 1	0.1935	0.036	2.2121	1.6061	Lower flange buckling
VT 12 20 2	0.2000	0.036	2.0606	1.6364	Lower flange buckling
VT 12 20 3	0.1865	0.036	1.8788	1.6061	Lower flange buckling
VT 12 30 1	0.1935	0.036	1.3636	1.3636	Lower flange buckling
VT 12 30 2	0.1745	0.036	1.5455	1.5152	Lower flange buckling
VT 12 30 3	0.1880	0.036	1.7273	1.6364	Lower flange buckling
VT 12 40 1	0.1755	0.036	1.5455	1.3333	Lower flange buckling
VT 12 40 2	0.1940	0.036	1.2121	1.1515	Lower flange buckling
VT 12 40 3	0.1955	0.036	1.2121	1.1515	Lower flange buckling

to define the real effective length, the subsequent scheme for the tested lattice joists will be considered (Figure 10).
For the scheme, a is a fixed dimension of 20 cm for all the present tests; v b is a measure dependent on c, and can be calculated by $b = 120 - a - 0,5.c$; c is the concrete opening value, taken either as 20, 30 or 40 cm in this research; pp is the lattice joist self

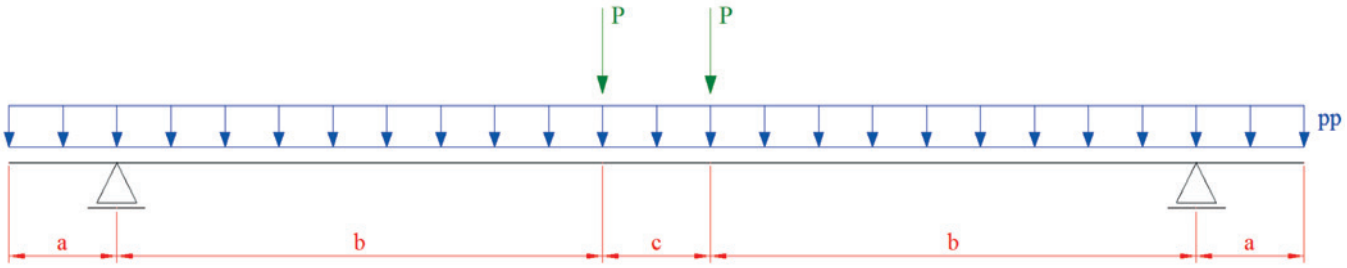

Figure 10
Static scheme of the tested lattice joists
Source: *Authors*

Table 2
Results for the negative bending tests (Part 2)

Modelo	pp (kN)	PD (kN)	$F_{failure}$ (kN)	F_{limit} (kN)	Failure mode
VT 16 20 1	0.2110	0.036	4.1212	2.6364	Lower flange buckling
VT 16 20 2	0.2060	0.036	3.5758	2.2424	Lower flange buckling
VT 16 20 3	0.2140	0.036	3.8788	2.6061	Lower flange buckling
VT 16 30 1	0.2140	0.036	2.6061	2.1818	Lower flange buckling
VT 16 30 2	0.2255	0.036	2.3030	2.2424	Lower flange buckling
VT 16 30 3	0.2165	0.036	2.5455	2.3333	Lower flange buckling
VT 16 40 1	0.1990	0.036	2.1515	2.1515	Lower flange buckling
VT 16 40 2	0.2045	0.036	2.1818	2.1818	Lower flange buckling
VT 16 40 3	0.2060	0.036	2.2727	2.2727	Lower flange buckling
VT 20 20 1	0.2290	0.036	3.2727	2.2121	Lower flange buckling
VT 20 20 2	0.2325	0.036	3.0000	2.0909	Lower flange buckling
VT 20 20 3	0.2365	0.036	3.6667	2.1818	Lower flange buckling
VT 20 30 1	0.2005	0.036	3.0000	3.5758	Lower flange buckling
VT 20 30 2	0.1915	0.036	3.4242	2.6970	Lower flange buckling
VT 20 30 3	0.2115	0.036	2.9394	2.6667	Lower flange buckling
VT 20 40 1	0.1840	0.036	2.5455	2.3333	Lower flange buckling
VT 20 40 2	0.2055	0.036	2.2424	2.1212	Lower flange buckling
VT 20 40 3	0.1970	0.036	2.0606	1.8485	Lower flange buckling
VT 25 20 1	Not used due to data error				
VT 25 20 2	0.2305	0.036	6.6970	2.5758	Diagonal buckling
VT 25 20 3	0.2365	0.036	6.9697	3.0909	Diagonal buckling
VT 25 30 1	0.2250	0.036	6.6667	3.0000	Lower flange buckling
VT 25 30 2	0.2225	0.036	4.9091	3.6364	Lower flange buckling
VT 25 30 3	0.2395	0.036	6.4545	2.7576	Lower flange buckling
VT 25 40 1	0.2240	0.036	4.8788	3.2727	Lower flange buckling
VT 25 40 2	0.2295	0.036	4.7879	3.4545	Lower flange buckling
VT 25 40 3	0.2300	0.036	4.9697	3.0000	Lower flange buckling
VT 30 20 1	0.2365	0.036	6.0606	3.5758	Diagonal buckling
VT 30 20 2	0.2325	0.036	6.3939	3.2727	Diagonal buckling
VT 30 20 3	0.2375	0.036	5.8788	3.5152	Diagonal buckling
VT 30 30 1	0.2435	0.036	6.3636	3.3030	Lower flange buckling
VT 30 30 2	0.2220	0.036	6.4242	3.6364	Lower flange buckling
VT 30 30 3	0.2170	0.036	6.3939	3.9091	Diagonal buckling
VT 30 40 1	0.2165	0.036	5.0000	3.4848	Lower flange buckling
VT 30 40 2	0.2160	0.036	4.9394	3.9394	Lower flange buckling
VT 30 40 3	0.2140	0.036	5.1818	4.0000	Lower flange buckling

pp – self weight; PD – test equipment weight; F_{limit} – equivalent load for a 4 mm displacement (ℓ/500); $F_{failure}$ – buckling load for any of the lattice joist elements or welded node rupture.

weight action divided by 240 cm (Table 2); and P is the applied load ($F_{failure}$) added to the weight of the test equipment (PD) (Table 2) divided by 2.

The maximum bending moment and shear force acting on each joist can be calculated for the scheme illustrated in Figure 10. The maximum values of the bending moment $M_{máx}$ (middle joist span) and shear force $V_{máx}$ (internally to any of the supports) can be calculated by Equations 3 and 4.

$$M_{máx} = \frac{pp.c^2}{8} + \left[P + pp.\left(a + b + \frac{c}{2}\right)\right].b - pp.a.\left(\frac{a}{2} + b\right) \quad (3)$$

$$V_{máx} = P + pp.\left(b + \frac{c}{2}\right) \quad (4)$$

The results analysis is divided into three groups. The first one comprises the joists that failure for buckling in the lower flange, in the concrete opening region. The second group comprises the joists in which the failure occurred by the diagonal buckling. Finally, the third one discusses the results regarding the deflections.

4.1 Failure due to buckling of the lower flange

The maximum bending moment and internal forces in the truss are shown in Figure 11.

Where h is the height of the truss; R_c is the compression force resulting in the lower flange; and R_t is the tension force resulting in the upper flange.

The value of R_c is determined by Equation 5.

$$R_c = \frac{M_{max}}{h} \quad (5)$$

As the lower flange is composed by 2 steel bars, the resulting compression force acting in one of the bars (F_c) in given by Equation 6.

$$F_c = \frac{R_c}{2} \quad (6)$$

The Euler critical buckling load (P_{cr}) for compressed elements is determined by Equation 7.

$$P_{cr} = \frac{\pi^2.E_s.I_{\phi,inf}}{l^2_{e,theoretical}} \quad (7)$$

where is the elasticity modulus of the steel truss taken as 21000 kN/cm²; $l_{e,theoretical}$ is the theoretical effective length of the bar; and v $I_{\phi,inf}$ is the gross moment of inertia of the lower flange (Equation 8).

$$I_{\phi,inf} = \frac{\pi.\phi^4_{inf}}{64} \quad (8)$$

where ϕ_{inf} is the diameter of one lower flange steel bar.

The monolithism provided by the welding in the truss nodes and the fixity of the bars in the concrete base shall interfere in the compressed elements effective buckling length. The lower flanges have theoretical effective lengths equal to 20, 30 and 40 cm – which refer to the concrete opening widths. If equal to P_{cr}, it is possible to calculate the real effective length ($l_{e,real}$) of the truss element (Equation 9).

$$l_{e,real} = \sqrt{\frac{\pi^2.E_s.I_{\phi,inf}}{F_c}} \quad (9)$$

The results of $l_{e,real}$ for the lattice joists that failure for lower flange buckling are summarized in Table 3, where 'Avrg' is the abbreviation for Average.

The ratio between the real effective length and the theoretical effective length is smaller than 1. It indicates that there is some stiffening in the lower truss bars possibly due to two reasons. One reason is related to the truss nodes, regarding the fact that an electro welded truss doesn't have fully pinned nodes, as it is considered in the classical mechanics. Another reason is related to the fixity of the lower bars to the concrete base of the joist. The lattice trusses

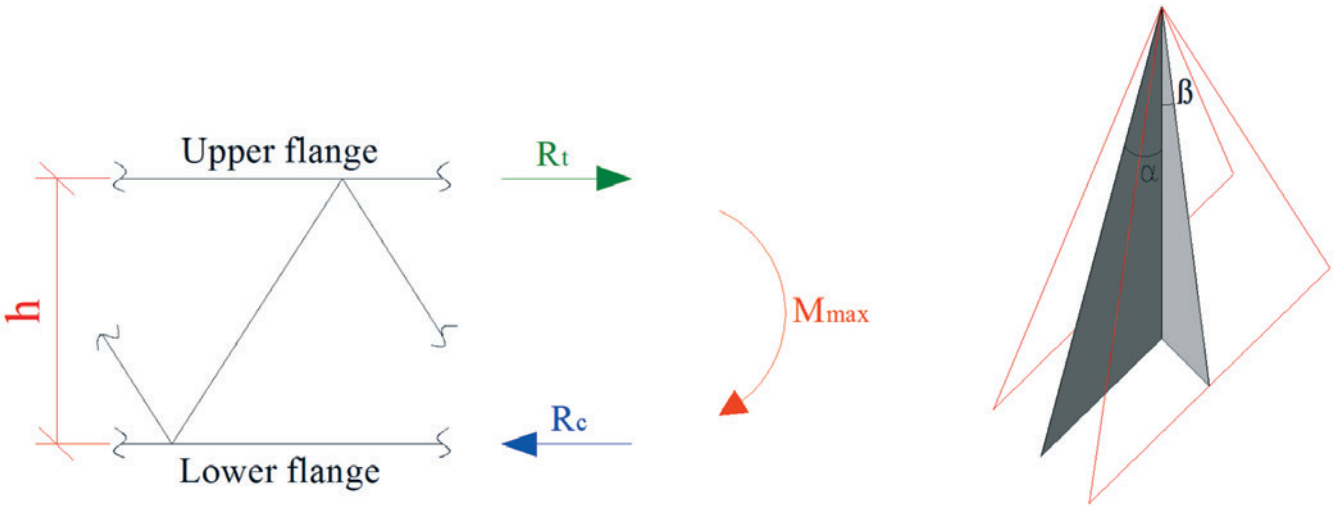

Figure 11
Resulting internal forces and bending moment in the truss
Source: *Authors*

with a height of 25 and 30 cm did not achieve lower flange failure, when the concrete opening was only of 20 cm. For these cases, the failure occurs in the diagonals.

4.2 Failure due to diagonal bars buckling

The maximum shear force in a lattice joist introduces compression stresses in its diagonals. The compression force (Q) in a truss diagonal is given by Equation 10.

$$Q = \frac{V_{max}}{4.\cos\alpha.\sin\beta} \quad (10)$$

where α and β are the truss angles, respectively defined by Equation 11 and 13:

$$\alpha = arctg\left(\frac{10}{h}\right) \quad (11)$$

$$\beta = arctg\left(\frac{z}{2.h}\right) \quad (12)$$

where h is the height of the truss in centimeters; z in the spacing between the two bars of the lower flanges, in centimeters, and is always the value of 9 cm for all the tested lattice joists.
When the compression force Q is equal to the Euler critical

Table 3
Values of $l_{e,real}$ for lattice joists with lower flange buckling failure

Model	$l_{e,real}$ (cm)	$l_{e,theoret}$ (cm)	$\frac{l_{e,real}}{l_{e,theoret}}$	Avrg
VT 06 20 1	6.88	20	0.34	0.35
VT 06 20 2	7.19	20	0.36	
VT 06 20 3	7.12	20	0.36	
VT 06 30 1	7.65	30	0.25	0.26
VT 06 30 2	7.72	30	0.26	
VT 06 30 3	7.81	30	0.26	
VT 06 40 1	8.04	40	0.2	0.21
VT 06 40 2	7.83	40	0.2	
VT 06 40 3	8.82	40	0.22	
VT 08 20 1	7.74	20	0.39	0.38
VT 08 20 2	7.70	20	0.39	
VT 08 20 3	7.24	20	0.36	
VT 08 30 1	8.65	30	0.29	0.29
VT 08 30 2	8.58	30	0.29	
VT 08 30 3	8.78	30	0.29	
VT 08 40 1	8.91	40	0.22	0.23
VT 08 40 2	9.62	40	0.24	
VT 08 40 3	9.19	40	0.23	
VT 10 20 1	8.51	20	0.43	0.42
VT 10 20 2	8.14	20	0.41	
VT 10 20 3	8.81	20	0.44	
VT 10 30 1	9.70	30	0.32	0.32
VT 10 30 2	Discarded			
VT 10 30 3	9.56	30	0.32	
VT 10 40 1	10.38	40	0.26	0.25
VT 10 40 2	9.68	40	0.24	
VT 10 40 3	10.27	40	0.26	
VT 12 20 1	8.38	20	0.42	0.43
VT 12 20 2	8.64	20	0.43	
VT 12 20 3	9.04	20	0.45	
VT 12 30 1	10.71	30	0.36	0.34
VT 12 30 2	10.18	30	0.34	
VT 12 30 3	9.65	30	0.32	
VT 12 40 1	10.49	40	0.26	0.28
VT 12 40 2	11.61	40	0.29	
VT 12 40 3	11.60	40	0.29	

Model	$l_{e,real}$ (cm)	$l_{e,theoret}$ (cm)	$\frac{l_{e,real}}{l_{e,theoret}}$	Avrg
VT 16 20 1	10.22	20	0.51	0.53
VT 16 20 2	10.94	20	0.55	
VT 16 20 3	10.51	20	0.53	
VT 16 30 1	13.03	30	0.43	0.44
VT 16 30 2	13.77	30	0.46	
VT 16 30 3	13.17	30	0.44	
VT 16 40 1	14.70	40	0.37	0.36
VT 16 40 2	14.59	40	0.36	
VT 16 40 3	14.32	40	0.36	
VT 20 20 1	12.71	20	0.64	0.63
VT 20 20 2	13.24	20	0.66	
VT 20 20 3	12.04	20	0.60	
VT 20 30 1	13.67	30	0.46	0.45
VT 20 30 2	12.86	30	0.43	
VT 20 30 3	13.78	30	0.46	
VT 20 40 1	15.25	40	0.38	0.40
VT 20 40 2	16.11	40	0.40	
VT 20 40 3	16.77	40	0.42	
VT 25 20 1	Not applicable			
VT 25 20 2				
VT 25 20 3				
VT 25 30 1	15.01	30	0.50	0.53
VT 25 30 2	17.39	30	0.58	
VT 25 30 3	15.23	30	0.51	
VT 25 40 1	17.97	40	0.45	0.45
VT 25 40 2	18.13	40	0.45	
VT 25 40 3	17.81	40	0.45	
VT 30 20 1	Not applicable			
VT 30 20 2				
VT 30 20 3				
VT 30 30 1	16.79	30	0.56	0.56
VT 30 30 2	16.74	30	0.56	
VT 30 30 3	16.78	30	0.56	
VT 30 40 1	19.47	40	0.49	0.49
VT 30 40 2	19.59	40	0.49	
VT 30 40 3	19.14	40	0.48	

Table 4
Values of $l_{e,real}$ for the lattice joists which presented a failure mode due to buckling of the diagonal bars

Model	$l_{e,real,d}$ (cm)	$l_{e,theoret,d}$ (cm)	$\frac{l_{e,real,d}}{l_{e,theoret,d}}$	Avrg
VT 25 20 1	Discarded			0.40
VT 25 20 2	10.99	27.30	0.40	
VT 25 20 3	10.78	27.30	0.39	
VT 25 30 1	11.02	27.30	0.40	0.43
VT 25 30 2	12.77	27.30	0.47	
VT 25 30 3	11.18	27.30	0.41	
VT 25 40 1	12.81	27.30	0.47	0.47
VT 25 40 2	12.92	27.30	0.47	
VT 25 40 3	12.69	27.30	0.46	

Model	$l_{e,real,d}$ (cm)	$l_{e,theoret,d}$ (cm)	$\frac{l_{e,real,d}}{l_{e,theoret,d}}$	Avrg
VT 30 20 1	10.67	31.94	0.33	0.33
VT 30 20 2	10.40	31.94	0.33	
VT 30 20 3	10.82	31.94	0.34	
VT 30 30 1	10.41	31.94	0.33	0.33
VT 30 30 2	10.38	31.94	0.33	
VT 30 30 3	10.41	31.94	0.32	
VT 30 40 1	11.71	31.94	0.37	0.37
VT 30 40 2	11.78	31.94	0.37	
VT 30 40 3	11.52	31.94	0.36	

buckling load P_{cr} (Equation 7), it is possible to obtain the real effective buckling length of the truss girder diagonals ($l_{e,real,d}$), given b Equation 13.

$$l_{e,real,d} = \sqrt{\frac{\pi^2 . E_s . I_{\phi,dig}}{Q}} \quad (13)$$

where $I_{\phi,dig}$ is the moment of inertia of a diagonal bar (Equation 14).

$$I_{\phi,dig} = \frac{\pi . \phi_{dig}^4}{64} \quad (14)$$

where ϕ_{dig} is the diameter of the diagonal steel bar.
The diagonal theoretical effective buckling length ($l_{e,theoretical,d}$) is determined by Equation 15, in centimeters.

$$l_{e,theoretical,d} = \sqrt{\left(\frac{z}{2}\right)^2 + h^2 + 100} \quad (15)$$

From Equations 13 and 15 it is possible to calculate the ratio between real and theoretical effective length. Results for the samples that failure of the lattice joist was due to buckling of the diagonals are presented in Table 4. The results are regarding to trusses with heights of 25 and 30 cm, as far as the failure mode described in this item only occurred for these geometry. For other values of height, the buckling of diagonal bars is not the predominant failure mode for the proposed test set-up.
The fixity of the welded nodes and the embedment of the diagonal bars in the joist concrete strongly reduce the effective buckling length of the diagonal bars.

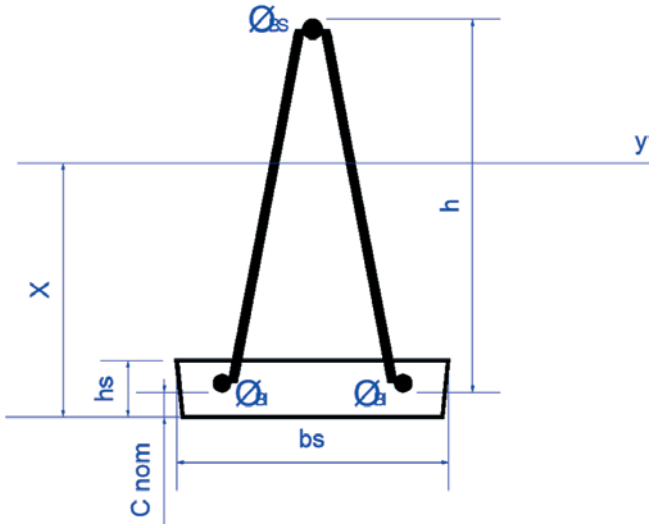

Figure 12
Joist cross section
Source: *Authors*

4.3 Deflection analysis

The deflection calculation is particularly complex in the step of analysis of results due to the composite cross section of the lattice joist – one of the section regions is composed by concrete and steel, while the other one is only composed by the steel truss bars. The moments of inertia are calculated separately for each region of the cross section mentioned above (Equations 16 to 22).
Properties of the transformed section

$$\alpha_e = \frac{E_s}{E_{cs}} \quad (16)$$

$$x = \frac{\left[\frac{\phi_{BS}^2}{4} . \left(h - \frac{\phi_{BS}}{2} + c_{nom}\right) + \frac{\phi_{BI}^2}{2} . \left(\frac{\phi_{BI}}{2} + c_{nom}\right)\right] . \pi . \alpha_e + \frac{h_s^2 . b_s}{2}}{\left(\frac{\phi_{BS}^2}{4} + \frac{\phi_{BI}^2}{2}\right) . \pi . \alpha_e + h_s . b_s} \quad (17)$$

$$I_H = \frac{\pi . \phi_{BS}^4}{64} + \frac{\pi . \phi_{BI}^4}{32} + \left[\frac{\phi_{BS}^2}{4} . \left(h + c_{nom} - x - \frac{\phi_{BS}}{2}\right)^2 + \frac{\phi_{BI}^2}{2} . \left(x - \frac{\phi_{BI}}{2} - c_{nom}\right)^2\right] . \quad (18)$$

$$\pi . \alpha_e + + \frac{h_s^3 . b_s}{12} + h_s . b_s . \left(x - \frac{h_s}{2}\right)^2$$

The parameters indicated in Equations 16 and 18 are shown in Figure 12: x is the distance from the center of gravity position (of the transformed cross section) to the bottom face of the section;

I_H is moment of inertia of the transformed cross section; ϕ_{BS} is the diameter of the upper flange bar;
ϕ_{BI} is the diameter of the lower flange bars; h is the height of the lattice truss; c_{nom} is the concrete cover for the lower flange bars, always equal to 1.5 cm along this research; b_s is the width of the concrete joist base, always equal to 12.0 cm for the present tests; h_s is the height of the concrete, taken as 2.5 cm in this research; α_e is the ratio between the steel modulus of elasticity (E_s) taken as 21000 kN/cm², and the concrete secant modulus of elasticity (E_{cs}) given by Equation 19.

$$E_{cs} = \alpha_i . E_{ci} \tag{19}$$

where E_{ci} is the tangent modulus of elasticity of the concrete; α_i is a parameter defined by Equation 20, which depends on the characteristic compressive concrete strength $f_{ck}\,(MPa)$. As mentioned before, the E_{ci} value is approximately 20% to 40% smaller than the dynamic elasticity modulus. In this article, the elasticity modulus values presented in Table 1 were reduced in 30% in order to correlate the dynamic and static modulus of elasticity.

$$\alpha_i = 0{,}8 + 0{,}2.\frac{f_{ck}}{80} \leq 1{,}0 \tag{20}$$

Properties of the section composed only for the steel truss bars

$$x_1 = \frac{\frac{\pi.\phi_{BI}^3}{4} + \frac{\pi.\phi_{BS}^2}{4}.\left(h - \frac{\phi_{BS}}{2}\right)}{\frac{\pi.\phi_{BI}^2}{2} + \frac{\pi.\phi_{BS}^2}{4}} \tag{21}$$

$$I_s = \left[\frac{\pi.\phi_{BS}^4}{64} + \frac{\pi.\phi_{BS}^2}{4}.\left(h - x_1 - \frac{\phi_{BS}}{2}\right)^2\right] + 2.\left[\frac{\pi.\phi_{BI}^4}{64} + \frac{\pi.\phi_{BI}^2}{4}.\left(x_1 - \frac{\phi_{BI}}{2}\right)^2\right] \tag{22}$$

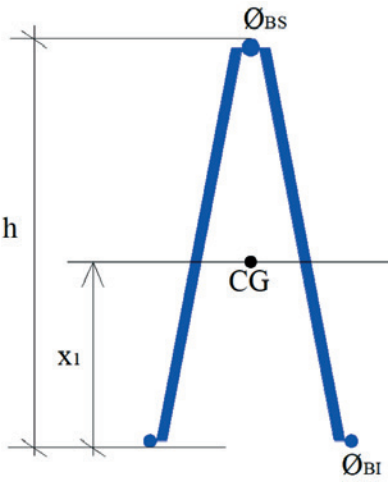

Figure 13
Center of gravity position for the lattice truss steel elements
Source: *Authors*

According to the Figure 13, the parameters used in Equations 21 and 22 are: x_1 is the distance between the center of gravity of the section and its bottom base; I_S is the moment of inertia of the steel section; ϕ_{BS} is the diameter of the upper flange bar; ϕ_{BI} is the diameter of the lower flange bars; h is the height of the lattice truss. Considering Figure 10, it is observed that for *a* e *b* segments the moment of inertia is equal to $\boldsymbol{I_H}$, whereas the moment of inertia is equal to $\boldsymbol{I_s}$ for segment *c*. The values for the experimental deflection are taken in the application load points (P). Therefore, the theoretical deflection value, analyzing the same point, is given by Equation 23.

$$a_P = -\frac{1}{(E_{cs}.I_H)theoretical}.\left\{\begin{array}{l} -\frac{pp.a^2.b^2}{4} - \frac{pp.a.b^3}{6} - \frac{pp.b^4}{24} + \frac{R.b^3}{6} + \\ \frac{pp.a^2.b}{2} + \frac{pp.a.b^2}{2} + \frac{pp.b^3}{6} - \frac{R.b^2}{2} + \\ +b.\left[+\frac{(E_{cs}.I_H)_{theoretical}}{(E_s.I_s)_{theoretical}}.\left(\begin{array}{l} -\frac{pp.c.(a^2+b^2)}{4} - \frac{pp.a.b.c}{2} + \\ -\frac{pp.c^2.(a+b)}{8} - \frac{pp.c^3}{48} + \\ -\frac{F_{lim}.c^2}{16} + \frac{R.b.c}{2} + + \frac{R.c^2}{8} \end{array}\right)\right] \end{array}\right\} \tag{23}$$

Rewriting the expression, Equation 24 is obtained.

$$a_P = -\frac{1}{(E_{cs}.I_H)theoretical}.\left[\frac{pp.a^2.b^2}{4} + \frac{pp.a.b^3}{3} + \frac{pp.b^4}{8} - \frac{R.b^3}{3}\right] + -\frac{1}{(E_{cs}.I_H)theoretical}.\left(\begin{array}{l} -\frac{pp.b.c.(a^2+b^2)}{4} - \frac{pp.a.b^2.c}{2} - \frac{pp.b.c.(a+b)}{8} + \\ -\frac{pp.b.c^3}{48} - \frac{F_{lim.b.c^2}}{16} + \frac{R.b^2.c}{2} + \frac{R.b.c^2}{8} \end{array}\right) \tag{24}$$

$$R = \frac{F_{lim}}{2} + pp.\left(a + b + \frac{c}{2}\right) \tag{25}$$

where $\left(E_{cs}.I_H\right)_{theoretical}$ is the theoretical stiffness of the transformed joist and $\left(E_s.I_s\right)_{theoretical}$ is the theoretical stiffness of the lattice truss steel section. If a_P is equal to the limit deflection a_{lim}, Equation 26 is obtained.

$$(E_{cs}.I_H)_{real} = \frac{\left[-\frac{pp.a^2.b^2}{4} - \frac{pp.a.b^3}{3} - \frac{pp.b^4}{8} + \frac{R.b^3}{3}\right]}{0{,}40 + \frac{1}{(E_s.I_s)_{theoretical}}.\left(\begin{array}{l} -\frac{pp.b.c(a^2+b^2)}{4} - \frac{pp.a.b^2.c}{2} \\ -\frac{pp.b.c^2.(a+b)}{8} + \\ -\frac{pp.b.c^3}{48} - \frac{F_{lim}.b.c^2}{16} + \\ \frac{R.b^2.c}{2} + \frac{R.b.c^2}{8} \end{array}\right)} \tag{26}$$

$\left(E_{cs}.I_H\right)_{real}$ is the mean stiffness of the testes joist that will be used for the deflection calculation. This stiffness is different from the theoretical stiffness due to the concrete cracking. Table 5 presents the results of the deflection values. It can be seen that the real

stiffness $\left(E_{cs}.I_H\right)_{real}$ is much smaller than the theoretical one. The discontinuity occasioned by the concrete opening and the concrete cracking explain this reduction. In the theoretical calculation, the value for the neutral axis position results in some point close to the concrete footing, indicating that concrete cracking is occurring.

5. Results applicability

As mentioned in item 1, during the assembly of a cantilever slab with concrete opening in the region right over the supports, there is a need of knowing the lattice joist strength during the construction phase. In this phase, the lattice joist will support itself the weight of the fresh concrete, of the workers and of the concreting equipment. The failure modes visually observed in the tests were: lower flange buckling due to hogging moments and diagonal bars buckling due to shear forces. Besides this modes of failure, it can still occur the failure of the welded node due to shear forces.

When a joist, mini panel or panel is loaded and positioned over the supports, bending moments and shear loads will develop. For cases of sagging moments acting on the structure, the adequate equation can be found in Sartorti *et al* [3]. For cases of hogging moments acting on the structure in regions where a concrete opening exists, the present article defines equations for calculating the resisting hogging moment and shear forces.

Table 5
Results of deflection values

Model	Concrete mixture	$(E_{cs}.I_H)_{real}$	$\frac{(E_{cs}.I_H)_{real}}{(E_{cs}.I_H)_{theoret}}$	Avrg
VT 06 20 1	14	155321.61	0.68	0.67
VT 06 20 2	15	153670.84	0.67	
VT 06 20 3	15	153898.86	0.67	
VT 06 30 1	14 e 15	109085.05	0.48	0.47
VT 06 30 2	14	106071.52	0.46	
VT 06 30 3	14	106001.81	0.46	
VT 06 40 1	14	81921.97	0.36	0.35
VT 06 40 2	15	81117.07	0.36	
VT 06 40 3	13 e 14	76077.79	0.33	
VT 08 20 1	13	244466.56	0.64	0.63
VT 08 20 2	13	225608.62	0.59	
VT 08 20 3	13	246429.20	0.65	
VT 08 30 1	13	163054.65	0.43	0.42
VT 08 30 2	13	164707.40	0.43	
VT 08 30 3	13	156758.64	0.41	
VT 08 40 1	12	125388.10	0.33	0.32
VT 08 40 2	12	118529.19	0.31	
VT 08 40 3	12	118798.22	0.31	
VT 10 20 1	8	292534.04	0.51	0.51
VT 10 20 2	8	288632.99	0.50	
VT 10 20 3	8	302612.31	0.53	
VT 10 30 1	9	212033.91	0.37	0.36
VT 10 30 2	9	Discarded		
VT 10 30 3	9	211147.67	0.36	
VT 10 40 1	10	159338.07	0.27	0.28
VT 10 40 2	10	171124.24	0.29	
VT 10 40 3	10	161330.79	0.28	
VT 12 20 1	11	364945.36	0.44	0.45
VT 12 20 2	11 e 12	369795.56	0.45	
VT 12 20 3	12	364380.21	0.44	
VT 12 30 1	11	252972.47	0.31	0.33
VT 12 30 2	11	267979.65	0.33	
VT 12 30 3	11	280947.89	0.34	
VT 12 40 1	10	195258.00	0.24	0.23
VT 12 40 2	10 e 11	180423.56	0.22	
VT 12 40 3	10	180503.02	0.22	

Model	Concrete mixture	$(E_{cs}.I_H)_{real}$	$\frac{(E_{cs}.I_H)_{real}}{(E_{cs}.I_H)_{theoret}}$	Avrg
VT 16 20 1	6	655614.76	0.35	0.34
VT 16 20 2	6	580841.79	0.31	
VT 16 20 3	6	650375.24	0.35	
VT 16 30 1	7	450662.25	0.24	0.25
VT 16 30 2	7	460356.94	0.25	
VT 16 30 3	7	472568.42	0.25	
VT 16 40 1	8	355565.70	0.19	0.19
VT 16 40 2	8	359303.44	0.19	
VT 16 40 3	7	369402.60	0.20	
VT 20 20 1	5	622823.28	0.21	0.21
VT 20 20 2	4	595495.63	0.20	
VT 20 20 3	5	616838.05	0.21	
VT 20 30 1	5	717295.38	0.24	0.21
VT 20 30 2	5	580981.72	0.20	
VT 20 30 3	5	577835.01	0.20	
VT 20 40 1	6	419473.45	0.14	0.13
VT 20 40 2	6	392026.70	0.13	
VT 20 40 3	6	352356.85	0.12	
VT 25 20 1	1	Discarded		0.18
VT 25 20 2	1	757046.84	0.16	
VT 25 20 3	1	885769.99	0.19	
VT 25 30 1	1	702880.20	0.15	0.16
VT 25 30 2	2	822666.67	0.18	
VT 25 30 3	1 and 2	657050.13	0.14	
VT 25 40 1	2	614253.09	0.13	0.13
VT 25 40 2	2	641758.34	0.14	
VT 25 40 3	2	573322.11	0.12	
VT 30 20 1	3	1052186.65	0.13	0.12
VT 30 20 2	3	972026.25	0.12	
VT 30 20 3	3	1036486.34	0.12	
VT 30 30 1	3	809006.88	0.10	0.10
VT 30 30 2	3	876744.26	0.10	
VT 30 30 3	4	932740.84	0.11	
VT 30 40 1	4	857489.47	0.10	0.10
VT 30 40 2	4	768769.84	0.09	
VT 30 40 3	4	778578.07	0.09	

5.1 Lower flange buckling due to hogging moments

The Equations 27 to 30 are deduced and based on the prior equations presented in this paper. The resisting bending moment (negative bending moment) is defined by Equation 29.

$$M_{d,res} = P_{CR}.h \quad (27)$$

$$P_{CR} = \frac{2.\pi^2.E_s.I_{\phi,inf}}{l^2_{e,real}} \quad (28)$$

$$M_{d,res} = \frac{2.\pi^2.E_s.I_{\phi,inf}}{l^2_{e,real}}.h \quad (29)$$

$$l_{e,real} = l_{e,theorical}.Avrg \quad (30)$$

Where P_{CR}. is the critical buckling load in the lower flange; h is the height of the truss; E_s is the steel modulus of elasticity; $I_{\phi,inf}$ is the moment of inertia of the lower bars cross section; $l_{e,real}$ is the real effective buckling length of the lower flange at the concrete opening; $l_{e,theorical}$ is the theoretical buckling effective length of the lower flange at the concrete opening – which can measure 20, 30 or 40 cm; $Avrg$ is the indicated in the last column of Table 3.
Structural safety is guaranteed when the following condition is satisfied (Equation 31):

$$M_{d,res} \geq M_{Sd} \quad (31)$$

Where M_{Sd} is the design bending moment.

5.2 Diagonal bars buckling due to shear

The axial force (Q) that compresses a diagonal bar is given by Equation 10. For obtaining Equation 32, the value of V_{max} was replaced by the design shear force V_{Sd}, in Equation 10.

$$Q = \frac{V_{Sd}}{4.\cos\alpha.\sin\beta} \quad (32)$$

The axial critical buckling load ($P_{CR,D}$) of a diagonal bar is defined by Equations 33 and 34.

$$P_{CR,D} = \frac{\pi^2.E_s.I_{\phi,dig}}{l^2_{e,real,d}} \quad (33)$$

$$l_{e,real,d} = l_{e,theorical,d}.Avrg \quad (34)$$

where E_s is the steel modulus of elasticity; $I_{\phi,dig}$ is the moment of inertia of the diagonal bar cross section; v is the real effective buckling length of the diagonal bar; $l_{e,theorical,d}$ is the theoretical buckling effective length of the diagonal bar; $Avrg$ is the value indicated in the last column of Table 4.
Structural safety is guaranteed when the following condition is satisfied (Equation 35):

$$P_{CR,D} \geq Q \quad (35)$$

5.3 Failure of the welded node

The upper node shear force resistance (V) shall meet the requirement of Equation 36, adapted from ABNT NBR 14862 [1].

$$V = \frac{15.\pi.\phi^2_{BS}.h}{4.l_{node}} \quad (36)$$

where ϕ_{BS} is the diameter of the upper flange bar; h is the height of the truss; l_{node} is the length between the truss nodes (defined as 20 cm); V_{Sd} is the design shear force in a transitory phase. Equation 37 shall be satisfied for safety guarantee.

$$V_{Sd} \leq V \quad (37)$$

5.4 Displacements calculation

In the transitory phase, it is recommended a limit value for the maximum displacement of the lattice joist, given by the span value divided by 500 ($l/500$). The stiffness values shall be calculated as indicated in Equation 38, using Equations 16 to 22.

$$(EI) = (EI)_{theorical}.Avrg = E_{CS}.I_H.Avrg \quad (38)$$

where E_{CS} is the secant modulus of elasticity of the concrete; I_H is the moment of inertia of the transformed section; $Avrg$ is the value indicated in the last column of Table 5.

6. Conclusions

In order to ease the construction of bridge decks, cantilever roofs and eaves, self-supporting lattice joists can be used working as formwork, capable of supporting its own weight, the fresh concrete weight and the weight workers and equipments in the construction phase.
This paper aimed to study the lattice joists behavior under negative bending moments, in cases where there is a concrete opening in the region of joist supports, by carrying out laboratory tests.
For lattice joists with a height of 20 cm or less, the predominant failure mode was the buckling of the lower flanges of the truss. In the cases of joists 25 or 30 cm height, with opening of 20 cm of the concrete, the buckling of diagonal bars governed the failure of the lattice joist. For the same truss height, considering the opening of 30 and 40 cm of the concrete, the lattice joist failure was governed by the lower flanges buckling.
The two mentioned modes of failure were analyzed separately for the calculation of the real effective buckling length. It was concluded that the diagonal and lower flange bars are stiffened by the electro welded truss nodes and by the fixity of the truss embedded in the concrete joist base. This results in a significant reduction of the effective buckling length. Disposing of the real effective buckling length, it is possible to calculate the maximum bending moments and shear forces resisted by the lattice joist. This values are quite important for the adequate design of the maximum cantilever span with no shuttering, or the maximum span between supports.
For the transition phase calculation, the stiffness value (EI) needs to be calibrated. It was verified that $(E_{CS}.I_H)_{real}$. is smaller than the theoretical value, due to discontinuity of the concrete in the base of the joist, and concrete cracking.

The equations for calculating resisting bending moments, shear strength and displacements are indicated in this paper. It is possible to define the maximum cantilever span or the maximum span between supports for a lattice joist with concrete opening, using the mentioned equation.

Studies about mini panels and latticed panels are recommended in order to check possible result variation. The present results show great load carrying capacity of the tested elements. It indicates that lattice joists with concrete opening shall be recommended for situations where monolithism between slabs and joists is desired, and less shuttering is needed, as expected in cases of bridge construction. It is important to emphasize that the present results cannot be extrapolated to models that were not tested, including other lattice joists with different geometry.

7. References

[1] ASSOCIAÇÃO BRASILEIRA DE NORMAS TÉCNICAS. NBR 14862. Armaduras treliçadas eletrossoldadas - Requisitos. Rio de Janeiro. 2002.

[2] _____NBR 14859-1. Laje pré-fabricada – Requisitos Parte 1: Lajes unidirecionais. Rio de Janeiro. 2002.

[3] SARTORTI, A. L.; FONTES, A. C.; PINHEIRO, L. M. Analysis of the assembling phase of lattice slabs. In: Revista IBRACON de Estruturas e Materiais. Volume 6, Number 4 (August 2013) p. 623-660. São Paulo: IBRACON, 2013.

[4] ASSOCIAÇÃO BRASILEIRA DE NORMAS TÉCNICAS. NBR 14859-2. Laje pré-fabricada – Requisitos Parte 2: Lajes bidirecionais. Rio de Janeiro. 2002.

[5] _____NBR 14860-1. Laje pré-fabricada – Pré-laje - Requisitos Parte 1: Lajes unidirecionais. Rio de Janeiro. 2002.

[6] _____NBR 14860-2. Laje pré-fabricada – Pré-laje - Requisitos Parte 2: Lajes bidirecionais. Rio de Janeiro. 2002.

[7] _____NBR 15696. Formas e escoramentos para estruturas de concreto – Projeto, dimensionamento e procedimentos executivos. Rio de Janeiro. 2009

[8] _____NBR 6118. Projeto de estruturas de concreto – Procedimento. Rio de Janeiro. 2014.

[9] SARTORTI, A. L.; VIZOTTO, I; PINHEIRO, L. M. Utilização de Minipainéis Treliçados para Construção de Tabuleiros de Pontes. Rio de Janeiro: IABSE, 2010.

[10] GASPAR, R. Análise da segurança estrutural das lajes pré-fabricadas na fase de construção. São Paulo, 1997. 103f. Dissertação (Mestrado em Engenharia de Estruturas)-Escola Politécnica da Universidade de São Paulo.

[11] TERNI, A. W.; MELÃO, A. R.; OLIVEIRA, L. E. A utilização do método dos elementos finitos na análise comportamental da laje treliçada na fase construtiva. Congresso Brasileiro do Concreto, 50. IBRACON. Salvador, 2008.

[12] AMERICAN SOCIETY FOR TESTING AND MATERIALS (ASTM). ASTM E1876-1: Standard test method for dynamic Young's modulus, shear modulus, and Poisson's ratio by impulse excitation of vibration. Philadelphia, 2005.

[13] SARTORTI, A. L. Comportamento dinâmico de lajes maciças de concreto leve com pérolas de EPS. 2015. 215p. Tese (Doutorado) – Departamento de Engenharia de Estruturas da escola de engenharia de São Carlos da Universidade de São Paulo, São Carlos, 2015.

[14] METHA, P. K.; MONTEIRO, P. J. M. Concreto: microestrutura, propriedade e matérias. 2 ed. São Paulo: IBRACON, 2014.

[15] FUSCO, P. B. Tecnologia do concreto estrutural: tópicos aplicados. São Paulo: Pini, 2008.